

CrystEngComm

Accepted Manuscript



This is an *Accepted Manuscript*, which has been through the Royal Society of Chemistry peer review process and has been accepted for publication.

Accepted Manuscripts are published online shortly after acceptance, before technical editing, formatting and proof reading. Using this free service, authors can make their results available to the community, in citable form, before we publish the edited article. We will replace this *Accepted Manuscript* with the edited and formatted *Advance Article* as soon as it is available.

You can find more information about *Accepted Manuscripts* in the [Information for Authors](#).

Please note that technical editing may introduce minor changes to the text and/or graphics, which may alter content. The journal's standard [Terms & Conditions](#) and the [Ethical guidelines](#) still apply. In no event shall the Royal Society of Chemistry be held responsible for any errors or omissions in this *Accepted Manuscript* or any consequences arising from the use of any information it contains.

Cite this: DOI: 10.1039/c0xx00000x

www.rsc.org/xxxxxx

ARTICLE TYPE

High Quality β -FeOOH Nanostructures Constructed from Biomolecule-assisted Hydrothermal Approach and Their pH-responsive Drug Delivery Behaviors

Xinyu Zhang,^{#a} Juan Ge,^{#a} Bo Lei,^{*a} Yumeng Xue,^a and Yaping Du,^{*a}

Received (in XXX, XXX) Xth XXXXXXXXXX 20XX, Accepted Xth XXXXXXXXXX 20XX
DOI: 10.1039/b000000x

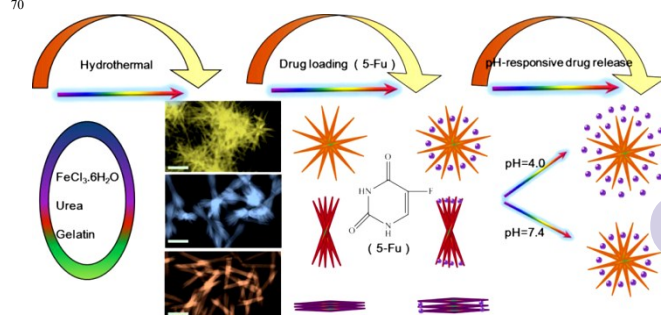
β -FeOOH nanostructures with diverse well-defined morphologies such as urchin-like, bowknot-like and bamboo leaves-like structures have been controllable synthesized from a facile gelatin-assisted hydrothermal approach. The as-obtained β -FeOOH nanostructures presented promising pH-controlled anti-cancer drug delivery behaviors and low-cytotoxicity and high cellular biocompatibility features.

Over the past few decades, there has been considerable interest in developing biocompatible nanomaterials as effective drug delivery vehicles.¹ Various nanomaterials have been used in drug delivery research fields as they can effectively deliver drugs to target sites and thus increasing the therapeutic benefit while minimizing the side effects.² To efficiently increase the nanomaterials therapeutic ability, the smart nanostructures with environmental responses including temperature, magnetic field, enzymatic activities as well as pH value have been designed and explored for potential biomedical applications.^{3–5} Among these stimuli, pH-response has been widely employed to design novel smart nanomaterials for drug delivery and disease therapy.⁶ Due to the various pH gradients in human tissues and cells such as stomach lumen (pH 1–3), ileum (pH 6.6–7.5), tumors (pH 5.7–7.8) and intracellular cancer cells (pH<6), it is very promising by adopting pH-responsive nanostructures as drug carrier for cancer therapy.^{7–9}

β -FeOOH (Akaganeite), with a hollandite-type structure, in which the iron atoms are strongly bonded to the framework that constitutes the tunnels, is an important semiconductor with the band gap of ~ 2.12 eV. β -FeOOH materials have stirred up great research interest in their nanoscale counterparts and applied in the area of magnetic storage devices, catalysis, sensors, and high-sensitivity bimolecular magnetic resonance imaging (MRI) for medical diagnosis and therapeutics.^{10–12} Moreover, β -FeOOH nanostructures with low toxicity have been recently explored for related biomedical applications.^{13–15}

Up to now, several research groups have explored the controlled synthesis of β -FeOOH nanostructures via wet-chemistry approaches as well as their material properties. For example, Bakoyannakis et al. prepared β -FeOOH nanoparticles by hydrolysis of ferric chloride hydrates ($\text{FeCl}_3 \cdot 6\text{H}_2\text{O}$) in the ammonium carbonate ($(\text{NH}_4)_2\text{CO}_3$) medium,¹⁶ by employing the same strategy, but hydrolysis of ferric chloride (FeCl_3) in the

ammonium hydroxide ($\text{NH}_3 \cdot \text{H}_2\text{O}$) and ethylene diamine tetraacetic acid (EDTA) solutions, Mohapatra et al. attained β -FeOOH nanorods and studied the related material absorptive behaviors,¹⁷ and Zeng et al. synthesized β -FeOOH nanospindles by co-hydrolysis of ferric chloride (FeCl_3) and ferrous chloride (FeCl_2) precursors in the presence of cetyltrimethyl ammonium bromide (CTAB) and investigated their magnetic resonance imaging applications.¹⁸ Jia et al. obtained the β -FeOOH nanorods through hydrothermal reaction of $\text{FeCl}_3 \cdot 6\text{H}_2\text{O}$ and urea in the presence of ethylene glycol (EG) surfactant and studied their ion-exchange properties.¹⁹ Xie et al. fabricated oriented β -FeOOH nanowires arrays by thermolysis of ferroin ($[\text{Fe}(\text{phen})_3]^{2+}$) and probed into their electrochemical properties.²⁰ Kim et al. fabricated β -FeOOH nanoparticles through the precipitation of ferric ions in a two-phase liquid system in the existence of sodium oleate and investigated their arsenic removal applications.²¹ However, to our best knowledge, a systematical controlled synthesis of high quality (pure phase, monodisperse and well-defined morphology) β -FeOOH nanostructures and exploration of their corresponding materials' applications have not been demonstrated, which inspires the continuous and systematic exploration.



Scheme 1 The schematic illustration of formation β -FeOOH nanostructures, and pH-responsive anti-cancer drug delivery application (Scale bar: 500 nm).

In this report, for the first time, we established a facile and effective approach for one pot synthesis of high quality β -FeOOH nanostructures with diverse morphologies, namely **FeOOH1** with urchin-like structure, **FeOOH2** with bowknot-like structure, and **FeOOH3** with bamboo leaves-like structure, in which by employing ferric chloride hydrates ($\text{FeCl}_3 \cdot 6\text{H}_2\text{O}$) and urea as

precursors and gelatin as surfactant. Due to their low toxicity and good stability properties, as a proof of concept, these different morphological β -FeOOH nanostructures showed promising pH-controlled anti-cancer drug delivery behaviors (Scheme 1).

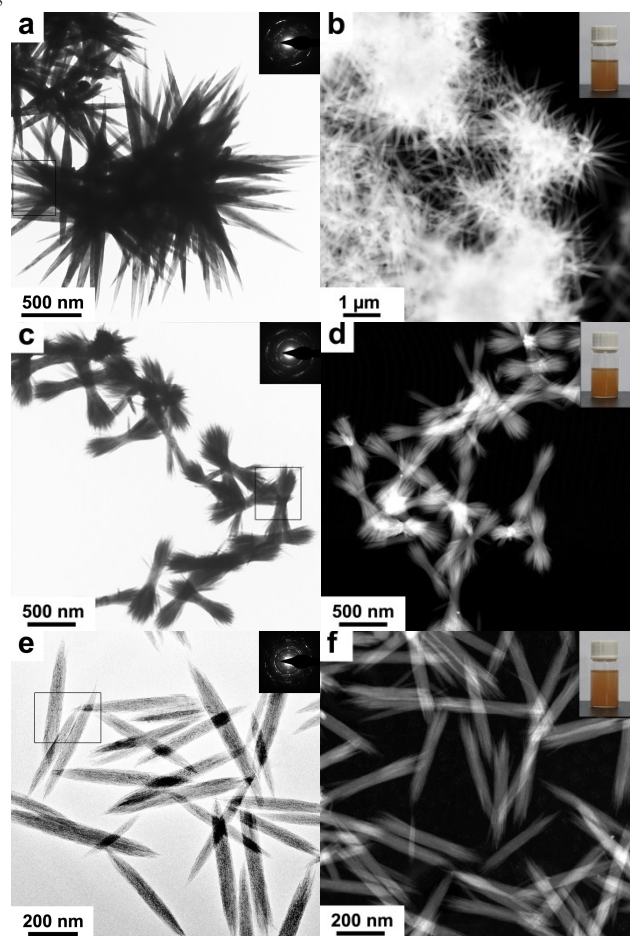


Fig. 1 TEM and HAADF-STEM images of (a, b) **FeOOH1**, (c, d) **FeOOH2**, and (e, f) **FeOOH3** samples. Insets of Fig. 1a, 1c, and 1e are the SAED patterns for three representative β -FeOOH samples (the highlighted black area). Insets of Fig. 1b, 1d, and 1f are the photographs of colloid β -FeOOH samples dispersed in ethanol, which have been placed in an ambient environment for more than 1 month.

The morphologies of the as-obtained β -FeOOH nanostructures were observed by transmission electron microscopy (TEM) and high-angle annular dark field-scanning transmission electron microscopy (HAADF-STEM). Based on the TEM and HAADF-STEM characterizations, three different morphologies of β -FeOOH nanostructures were obtained in the present one pot synthesis, importantly, the as-synthesized β -FeOOH nanostructures are monodispersibility without further size and shape sorting process. For example, under the conditions of 100 mmol of $\text{FeCl}_3 \cdot 6\text{H}_2\text{O}$ and 100 mmol of urea in 9 mL of gelatin were used for reaction at 80 °C for 21 h, the urchin-like β -FeOOH nanostructures, referred to as **FeOOH1**, were obtained (Fig. S1a† and Fig. 1a and 1b). Fig. S1a† exhibited a typical low magnified TEM image of the as-obtained **FeOOH1** product composed of many urchin-like microspheres. The detailed morphology of an individual urchin-like structure was shown in the Fig. 1a. It uncovered that the entire structure was comprised

of numerous solid nanoneedles with lengths of average \sim 500 nm, and the nanoneedles connected to each other to form three dimensional (3D) hierarchical structures (Fig. 1a and 1b). The isolated dots form rings in the selected area electron diffraction (SAED) pattern (inset of Fig. 1a), demonstrating that the nanoneedles in the urchin-like **FeOOH1** microspheres were composed of highly crystalline nanocrystals.

Under the condition of 100 mmol of $\text{FeCl}_3 \cdot 6\text{H}_2\text{O}$ in 9 mL of gelatin were used for reaction at 80 °C for 23 h resulted in bowknot-like β -FeOOH nanostructures referred to as **FeOOH2** with average \sim 700 nm in length and \sim 100 nm in width at the knot position (Fig. S1b† and Fig. 1c and 1d). While under the condition of 300 mmol of $\text{FeCl}_3 \cdot 6\text{H}_2\text{O}$ and 100 mmol of urea in 9 mL of gelatin were used for reaction at 80 °C for 45 h led to the formation of bamboo leaves like β -FeOOH nanostructures referred to as **FeOOH3** with length of average \sim 500 nm in length and average \sim 50 nm in width (Fig. S1c† and Fig. 1e and 1f). The size distribution histogram of **FeOOH2** and **FeOOH3** nanostructures were also listed in Fig. S2a† and Fig. S2b†, respectively. Importantly, as seen from Fig. S1b† and S1c†, the as-harvested **FeOOH2** and **FeOOH3** were of high yields in morphologies. Digital photos demonstrated in inset of Fig. 1b, 1d and 1f showed the as-obtained β -FeOOH nanostructures are all readily dispersed and highly stable in polar solvents (e.g. ethanol) for more than 1 month and the SAED patterns shown in insets of Fig. 1c and 1d also opened out the good crystallinity of **FeOOH2** and **FeOOH3** samples.

Fig. 2a shows the X-ray diffraction patterns of the as-synthesized β -FeOOH products with different morphologies, and all the diffraction peaks can be indexed to a pure tetragonal phase (space group: $I4/m$ with lattice constants $a = 10.535$ Å, $b = 10.535$ Å, $c = 3.030$ Å, JCPDS: 34-1266). No diffraction peaks from any other chemical species such as α -FeOOH and γ -FeOOH were detectable. In addition, the broadening of the diffraction peaks suggested the nanocrystalline nature of the samples.

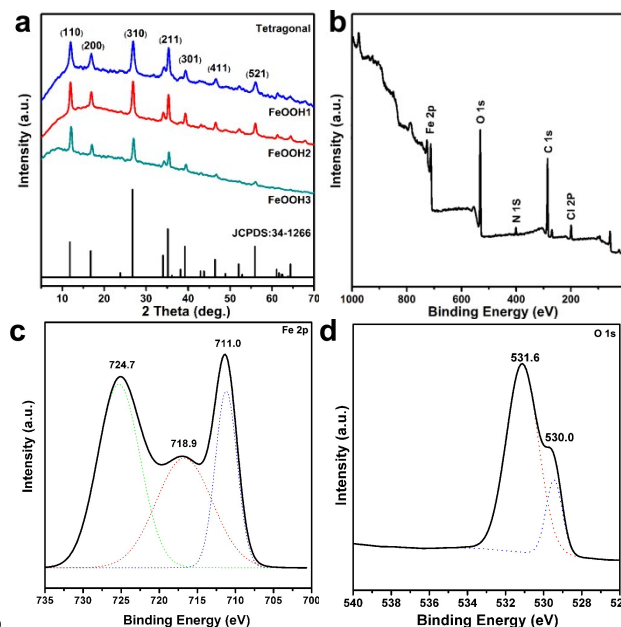


Fig. 2 (a) XRD patterns of as-prepared β -FeOOH nanostructures with different morphologies. XPS survey spectra (b) Fe 2p (c) and O 1s (d) of as-obtained β -FeOOH nanostructures.

X-ray photoelectron spectroscopy (XPS) analysis was adopted to further characterize the as-obtained β -FeOOH nanostructures. From Fig. 2b, peaks assignable to core levels of Fe 2p, O 1s, C 1s, N 1s, and Cl 2p were identified. The observable peaks ascribed to the core levels of N 1s and C 1s revealed the presence of gelatin ligands on the surfaces of nanostructures, the peak of Cl 2p suggested the presence of Cl atoms, which would be located in the hollandite channels of the β -FeOOH (Fig. S3†).²² Fig. 2c and 2d show the XPS spectra taken from the Fe 2p and O 1s regions of the β -FeOOH nanostructures. As seen from Fig. 2c, the double peaks at 711.0 eV and 724.7 eV are attributed to the core levels of Fe 2p_{3/2} and Fe 2p_{1/2}, respectively (a shakeup satellite at 718.9 eV can also be observed), indicating the presence of Fe (III) in β -FeOOH.²³ The XPS spectra of O 1s region with two-peak contribution illustrates that at least two kinds of oxygen species are present in the β -FeOOH sample (Fig. 2d). The peak at about 530.0 is due to crystal lattice oxygen of β -FeOOH, while the peak at about 531.6 eV is due to chemisorbed oxygen on the β -FeOOH surfaces.²⁴ The above results suggested that the oxidation states of iron ions are mainly trivalent for the β -FeOOH nanostructures, which is also in accord with the result of XRD characterization.

In this work, the controlled synthesis of high quality β -FeOOH nanostructures have been carefully conducted. Experimentally, we found that the quality of β -FeOOH nanostructures are mainly affected by reaction conditions, such as solvent composition, reaction temperature and time, the optimal synthetic parameters are screened so as to achieve the appropriate balance between the nucleation and growth stages of the crystals to obtain high quality products. Herein, taking **FeOOH1** as an example, if the amount of gelatin (1.0 g) and urea (100 mmol) were fixed, reaction at 80 °C for 21 h, when the content of FeCl₃·6H₂O was reduced from 100 mmol to 10 mmol, only aggregated **FeOOH1** nanoneedles with poor dispersibility were harvested (Fig. S4a†). Under the same reaction condition, except increasing FeCl₃·6H₂O content to 1 mol resulted in some unshapely urchin-like **FeOOH1** with low yields (Fig. S4b†). Besides the precursor concentrations, it was found that the volume of surfactants-gelatin was essential for the preparation of high-quality **FeOOH1** nanostructures. For instance, at a fixed experimental condition, by changing the gelatin from 0 g to 5 g, the unsystematic morphologies of **FeOOH1** were obtained (Fig. S5a† and S5b†). Notably, when using other type of gelatin (G2500-500G), a great amount of polydisperse nanoparticles were obtained (Fig. S5c†). In addition, we also found that both the reaction temperature and time remarkably affected the quality of the products. For example, at a fixed experimental condition, i.e. 100 mmol of FeCl₃·6H₂O, 100 mmol of urea 1.0 g of gelatin, reaction time kept for 21 h, when the reaction temperature was increased to 120 °C, the nanoneedles but with average ~500 nm length and ~50 nm diameter were assembled into 3D urchin-like nanostructures (Fig. S6a†), however, along with decrease of temperature to 40 °C, the non-uniform **FeOOH1** products with poor dispersibility were obtained (Fig. S6b†). On the other hand, at the fixed reaction temperature (i.e. 80 °C), the reaction of 100 mmol of FeCl₃·6H₂O, 100 mmol of urea and 1.0 g of gelatin, at a short reaction (t = 10 h) the as-obtained products were ill separated and coexisted with a great amount of irregular nanoparticles (Fig. S7a†). When prolonging the reaction time to 50 h, the 3D urchin-like **FeOOH1**

nanostructures further grown into aggregated 3D networks with board size distribution were obtained (Fig. S7b†). By conducting the same condition-based experiments, the controlled synthesis of high quality **FeOOH2** and **FeOOH3** nanostructures were also achieved (Fig. 1c and 1e).

To further characterize the as-obtained products, Fourier transform infrared (FTIR) spectroscopy of the β -FeOOH were recorded as shown in Fig. 3a. The characteristic bands located at 1630, 1380, and 890 cm⁻¹ were assigned to the Fe-O vibrational mode in β -FeOOH.²⁵ Therefore, the FTIR characterization also indicated that the as-obtained iron oxyhydroxides nanostructures were predominantly β -FeOOH, which was consistent with the XRD results. Nitrogen adsorption and desorption isotherm measurements were conducted to investigate the structure of the as-obtained β -FeOOH products. The specific surface areas were calculated based on the Brunauer–Emmett–Teller (BET) method.²⁶ As shown in Fig. 3b-d, the BET surface area of β -FeOOH nanostructures could be estimated to be 27.9 m²/g for **FeOOH1**, 70.8 m²/g for **FeOOH2**, and 42.8 m²/g for **FeOOH3** respectively. The high BET surface area endowed the as-obtained β -FeOOH nanostructures a promising candidate for application in drug delivery (Fig. S8† and Table 1).

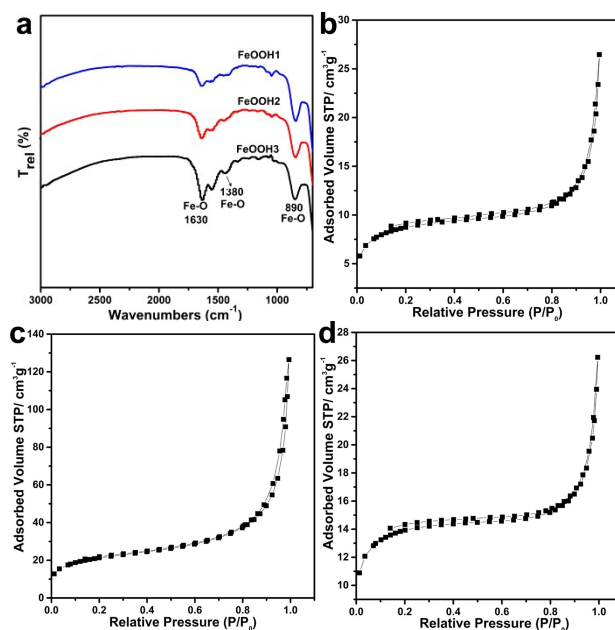


Fig. 3 (a) FTIR spectra of as-obtained β -FeOOH nanostructures. (b-d) Nitrogen adsorption-desorption isotherm for β -FeOOH nanostructures with different morphologies.

Table 1. Specific surface area, pore volume, pore size and drug loading efficiency of β -FeOOH nanostructures

Samples	Loading efficiency (%)	Specific surface area (m ² /g)	Pore volume (cm ³ /g)	Pore size (nm)
FeOOH1	3.12	27.9	0.03	4.12
FeOOH2	4.63	70.8	0.12	6.85
FeOOH3	2.72	42.8	0.03	2.96

As a proof of concept, after optimizing the experimental conditions (temperature, time and precursors concentration) the synthesized β -FeOOH nanostructures with urchin-like, bowknot-like and bamboo leaves-like structures were used as the drug delivery carriers and 5-Fluorouracil (5-Fu) (an anti-cancer drug) was loaded in their respective structures. The ultraviolet (UV)-vis absorption method was employed to determine the drug loading and releasing behaviors. The changes of UV-vis spectra of samples before and after drugs loading were shown in Fig. 4a. The characteristic peak identified at 266 nm was attributed to absorption of 5-Fu drug. After drug loading, the β -FeOOH nanostructures presented a typical characteristic peak located at 266 nm, suggesting the successful 5-Fu loading in samples. The further study showed that **FeOOH1**, **FeOOH2**, **FeOOH3** hold a drug loading efficiency of 3.12 %, 4.63 % and 2.72 %, respectively (Table 1). This drug loading capacity for our materials was comparable with the rare earth-based and iron oxide nanoparticles.^{27,28}

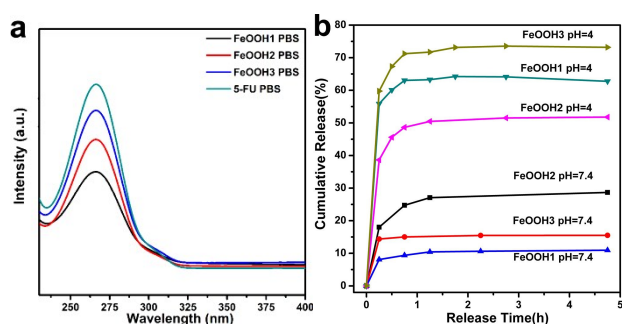


Fig. 4 Anti-cancer drug (5-Fu) loading and release evaluation. (a) UV-vis spectra of drug-loaded (5-Fu) β -FeOOH solution. (b) pH-responsive drug release behaviours at different pH medium.

compared with **FeOOH1** and **FeOOH3**, **FeOOH2** showed the low potential difference and then exhibited the fast drug release behaviors. On the other hand, at pH 4.0, due to the degradation of β -FeOOH, the specific surface area may play a leading role in controlling drug release instead of electrostatic interactions. **FeOOH2** had the high specific surface area and then showed slow release. The drug release behavior was usually influenced by the nanomaterials structures, drug loading as well as releasing medium. In our study, **FeOOH2** nanostructure has the highest specific surface area (70.8 m^2/g) compared to **FeOOH1** (27.9 m^2/g) and **FeOOH3** (42.8 m^2/g). Therefore, the high drug loading was observed for **FeOOH2** (4.63 %). Based on the high specific surface area and pore volume, the bowknot-like morphology (**FeOOH2**) showed a suitable pH-responsive drug release behavior, which may be a suitable nanostructure for drug delivery application. Taking account of the acidic environment in tumor cell, our pH-responsive system may act as a promising candidate for smart drug delivery and cancer therapy.

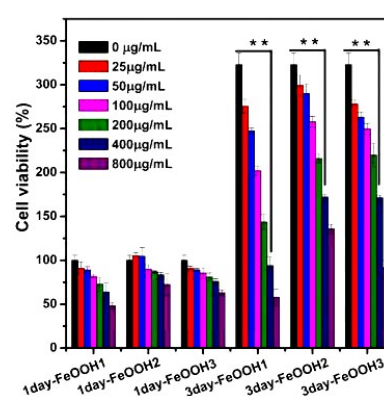


Fig. 5 Cell cytotoxicity assessment of β -FeOOH nanostructures with different morphologies. Cell viability of L929 cells treated with β -FeOOH nanostructures with different concentrations (25-800 $\mu\text{g/mL}$) was analysed after 1 and 3 days of incubation. ** $P < 0.01$ represents significant difference relative to the cell viability after culture for 1 day.

Cell cytotoxicity evaluation is very necessary before their further application in biomedicine. Therefore, we explored the effect of β -FeOOH nanostructures on fibroblasts (L929) viability shown in Fig. 5. In the culture periods of 1 and 3 days, L929 cells showed a significant proliferation after incubation with different concentrations of nanostructures (Fig. 5 and Fig. S9[†]). In the range from 25-200 $\mu\text{g/mL}$, the cell viability of L929 treated with **FeOOH2** and **FeOOH3** was comparable to the tissue culture plate (TCP) control, indicating their good cellular biocompatibility.

The anticancer ability of 5-Fu loaded β -FeOOH nanostructures was evaluated with human liver hepatocellular carcinoma cell line (HepG2 cells). Pure 5-Fu with different concentrations holds a significant killing ability against HepG2 cells (Fig. S10[†]). After incubation with β -FeOOH nanostructures with different concentrations (25-800 $\mu\text{g/mL}$) for 1 and 3 days, at least 75 % cells survived compared to TCP control, suggesting their low cytotoxicity. However, the cell viability of HepG2 cells decreased significantly when treated with 5-Fu loaded β -FeOOH nanostructures and only 35 % HepG2 cells survived with high concentrations of β -FeOOH nanostructures after 3 days incubation (800 $\mu\text{g/mL}$). These results indicated that β -FeOOH

nanostructures can be used in smart drug delivery and cancer therapy. In order to be used in anticancer applications, investigation on cellular uptake of β -FeOOH nanostructures is required. The fluorescent images of HepG2 cells after treated with Nile red-loaded nanoparticles are shown in Fig. S11[†]. The images showed that the β -FeOOH nanostructures could efficiently adhere to the cell surface and enter the cells, but they did not enter the cell nucleus. The test for L929 cell line showed the similar results (Fig. S12[†]). Due to the highly acidic environment, our pH-responsive β -FeOOH nanostructures may have promising application for drug delivery and cancer therapy.

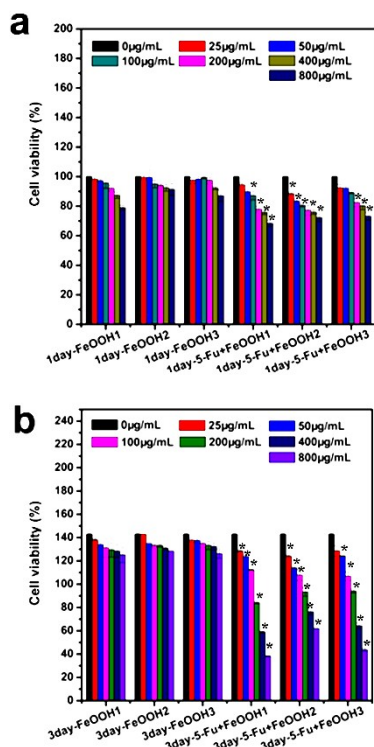


Fig. 6 Anticancer ability evaluation of 5-Fu loaded β -FeOOH nanostructures. (a-b) Cell viability of HepG2 cells treated with β -FeOOH nanostructures and 5-Fu loaded β -FeOOH nanostructures with different concentrations after 1 (a) and 3 days (b) of incubation. * $P < 0.05$ represents significant difference relative to the cell viability after culture with pure nanostructures.

Conclusions

In summary, we have successfully developed a simple gelatin-assisted hydrothermal method to synthesize high quality β -FeOOH nanostructures with diverse well-defined morphologies, i.e. urchin-like, bowknot-like and bamboo leaves-like structures. As a proof of concept, the as-obtained β -FeOOH nanostructures showed promising pH-controlled anti-cancer drug delivery behaviours. The cell cytotoxicity evaluation also demonstrated the low-cytotoxicity feature and high cellular biocompatibility. The drug-loaded β -FeOOH nanostructures could efficiently kill the HepG2 cancer cells. The excellent drug delivery properties and low-cytotoxicity features of the as-synthesized β -FeOOH nanostructures demonstrated that they may have great promise for

various biomedical applications such as smart drug delivery and cancer therapy.

Acknowledgements

We gratefully acknowledge the financial aid from the start-up founding from Xi'an Jiaotong University, the Fundamental Research Funds for the Central Universities (XJJ2014090, 1191320020), and the NSFC (Grant No. 21371140).

Notes and references

^a Frontier Institute of Science and Technology jointly with College of Science, State Key Laboratory for Mechanical Behavior of Materials, Xi'an Jiaotong University, 99 Yanxiang Road, Xi'an Shaanxi, 710054, China.

E-mail: ypdu2013@mail.xjtu.edu.cn; rayboo@mail.xjtu.edu.cn;

Tel&Fax: 86-29-83395385.

#These authors contributed equally.

[†] Electronic Supplementary Information (ESI) available: The experimental details, structural model, results of TEM, bioimaging are provided. See DOI: 10.1039/b000000x/

- [1] D. A. LaVan, T. McGuire and R. Langer, *Nat. Biotechnol.*, 2003, **21**, 1184–1191.
- [2] Q. A. Pankhurst, J. Connolly, S. K. Jones and J. Dobson, *J Phys D: Appl. Phys.*, 2003, **36**, R167–R181.
- [3] J. Akimoto, M. Nakayama and T. Okano, *J Controlled Release.*, 2014, **193**, 2–8.
- [4] D. Pan, C. Guo, K. Luo, Q. Yi and Z. Gu, *Biomaterials*, 2014, **35**, 10080–10092.
- [5] S. Mura, J. Nicolas and P. Couvreur, *Nat. Mater.*, 2013, **12**, 991–1003.
- [6] S. Wang, S. Zhang and J. Liu, *Appl. Surf. Sci.*, 2014, **6**, 10706–10713.
- [7] W. Gao, J. M. Chan and O. C. Farokhzad, *Mol. Pharm.*, 2010, **7**, 1913–1920.
- [8] C. H. Lee, S. H. Cheng and I. Huang, *Angew. Chem., Int. Ed.* 2010, **49**, 8214–8219.
- [9] P. He, S. Takeshima and S. Tada, *Vaccine*, 2014, **32**, 6199–6205.
- [10] L. P. Weng, W. H. Van Riemdsdijk and T. Hiemstra, *Environ. Sci. Technol.*, 2009, **43**, 7198–7204.
- [11] H. Marcussen, P. E. Holm, B. W. Strobel and H. C. B. Hansen, *Environ. Sci. Technol.*, 2009, **43**, 1122–1127.
- [12] T. Cheng, M. O. Barnett, E. E. Roden and J. L. Zhuang, *Environ. Sci. Technol.*, 2004, **38**, 6059–6065.
- [13] M. Kanematsu, T. M. Young, K. Fukushi, P. G. Green and J. L. Darby, *Environ. Sci. Technol.*, 2010, **44**, 3388–3394.
- [14] G. Ona-Nguema, G. Morin, F. Juillot, G. Calas and G. E. Brown, *Environ. Sci. Technol.*, 2005, **39**, 9147–9155.
- [15] D. A. Beattie, J. K. Chapelet, M. Grafe, W. M. Skinner and F. Smith, *Environ. Sci. Technol.*, 2008, **42**, 9191–9196.
- [16] E. A. Deliyanni, D. N. Bakoyannakis, A. I. Zouboulis, K. A. Matis and L. Nalbandian, *Microporous Mesoporous Mater.*, 2001, **42**, 49–57.
- [17] M. Mohapatra, L. Mohapatra, S. Anand and B. K. Mishra, *J. Chem. Eng. Data.*, 2010, **55**, 1486–1491.
- [18] L. Y. Zeng, W. Z. Ren, J. J. Zheng and A. G. Wu, *Appl. Surf. Sci.*, 2012, **258**, 2570–2575.
- [19] Y. X. Zhang and Y. Jia, *Appl. Surf. Sci.*, 2014, **290**, 102–106.
- [20] Y. Xiong, Y. Xie, S. W. Chen and Z. Q. Li, *Chem. Eur. J.*, 2003, **9**, 4991–4996.
- [21] K. H. Cho, B. Y. Shin, H. K. Park, B. G. Cha and J. Y. Kim, *RSC Adv.*, 2014, **4**, 21777–21781.
- [22] X. W. Song and J. F. Boily, *J. Phys. Chem. C*, 2012, **116**, 2303–2312.

-
- [23] L. L. Li, Y. Chu, Y. Liu and L. H. Dong, *J. Phys. Chem. C*, 2007, **111**, 2123–2127.
- [24] Y. P. Du, Y. W. Zhang, L. D. Sun and C. H. Yan, *J. Phys. Chem. C*, 2008, **112**, 12234–12241.
- 5 [25] X. W. Song and J. F. Boily, *J. Colloid Interface Sci.*, 2012, **376**, 331–333.
- [26] R. Cai, J. Chen, D. Yang, Z. Y. Zhang, S. J. Peng; J. Wu, W. Y. Zhang, C. F. Zhu, T. M. Lim, H. Zhang and Q. Y. Yan, *ACS Appl. Mater. Interfaces*, 2013, **5**, 10389–10394.
- 10 [27] C. Wang, L. Cheng and Z. Liu, *Biomaterials*, 2011, **32**, 1110–1120.
- [28] M. K. Yu, Y. Y. Jeong and J. Park, *Angew. Chem., Int. Ed.*, 2008, **47**, 5362–5365.